

Comparison of the Results of 2D and 3D Numerical Modeling of Flow over Spillway Chutes with Vertical Curvatures

Saeed-reza Sabbagh-yazdi,
Fateme Rostami, Habib Rezaei-manizani, and Nikos E. Mastorakis

Abstract— For flow conduits with mild slope and considerably large vertical curvatures the hydrostatic distribution of the pressure may be used for design purposes. However, for the spillway chutes actual pressure load over the steep slope beds with small vertical curvatures may differ from the hydrostatic pressure values. The differences in pressure load on curved bed chutes are mainly because of the centrifugal forces. In present work, the results of a version of the NASIR 2D Finite Volume flow solver which solves depth average flow equations on variable steep slope bed, are compared with the results of the Flow3D Finite Volume solver, which utilizes the VOF technique for solution of water free surface location as well as a set of laboratory measurements for test cases reported in the literature. The main goal of present work is to investigate the division of the numerically computed flow parameters (such as water surface elevation and bottom pressure) by 2D and 3D computational models from the hydrostatic assumptions

Keywords— Numerical Simulations, Flow parameters, Curved bed chutes.

I. INTRODUCTION

Rapidly varied transitions in open channels typically involve flows with high curvatures and or slop. The length of such transition is usually short and pressure distribution significantly non-hydrostatics and velocity distributions are highly non-uniform.

Manuscript received August 25, 2007; Revised received December 15, 2007. This work was supported in part by the Civil Engineering Department of K. N. Toosi University of Technology.

Saeed-Reza Sabbagh-Yazdi is with the Civil Engineering Department of K. N. Toosi University of Technology, No.1346 Valiasr Street, 19697- Tehran, IRAN (SYazdi@kntu.ac.ir).

Fateme Rostami, is with the Civil Engineering Department of K. N. Toosi University of Technology, No.1346 Valiasr Street, 19697- Tehran, IRAN (fa.rostami@gmail.com).

Habib Rezaei-Manizani, is with the Civil Engineering Department of K. N. Toosi University of Technology, No.1346 Valiasr Street, 19697- Tehran, IRAN (Rmanizani@yahoo.com).

NIKOS E. MASTORAKIS is with the Military Institutes of University Education (ASEI), Hellenic Naval Academy Terma Chatzikyriakou 18539, Piraeus, GREECE (mastor@wseas.org)

At present most computational modeling of open channel flows are based on the depth-averaged St. Venant equations, in these equations, a uniform longitudinal velocity and hydrostatic pressure distribution are assumed. Correction coefficients may be applied for different distributions if they can be established a priori (Yen 1973). These equations are applicable for very shallow flows, with wavelength-to-depth ratios in excess of about 20 (Henderson 1966). For moderately shallow flows (i.e., for shorter feature wavelengths), the Boussinesq equation are the next level of approximation (Chaudhry 1993). While the Boussinesq equation are applicable to somewhat shorter lengths (about six depths), they do not appear to have been successfully applied to problems with steep slopes (Montes 1994).

Dressler (1978) attempt to extend the one dimensional approach to higher-curvature flows by using a curvilinear, orthogonal coordinate system based on the bed geometry. This approach, applied by Sivakumaran et al. (1983), is based on a potential-flow assumption. The method, however does not account for the water-surface curvature being different from the bed curvature being different from the bed curvature and reduces to the St. Venant equation for a flat bed.

Hager and Hutter (1984) presented the method, based on potential flow in a streamline coordinate system, which assumes a linear variation of flow angle and curvature between the bed and surface. The result was shown to be an improvement over the Boussinesq equation but limited to geometrically mild slopes (up to about 60°). A similar but higher-order method was developed by Matthew (1991) in Cartesian coordinate system. This method involves an iterative solution. Corrections for the effect of friction were also incorporated.

A further alternative was presented by Steffler and Jin (1993). There, the plane Reynolds equation were vertically averaged, and moment equations were developed by vertically integrating the Reynolds equations after they had been multiplied by vertical coordinate. The three extra equations allow specification of three further flow parameters. Linear longitudinal velocities as well as quadratic-pressure and vertical-velocity distributions were assumed, and equations were rewritten in terms of parameters of these distributions. Essentially, the approach amounts to a low-order weighted residual method. The method suffers from the crudeness and

arbitrariness of the assumed distributions, and results in some long and complex equations where the terms are not of uniform order. It does have the advantage of incorporating the effect of turbulent stresses directly, although these are not important in the applications considered in this paper.

In this paper, a module of **FLOW-3D**[®], and a depth average version of **NASIR** flow solver are applied to model the free surface flow over the two small scale test cases. First, flow from horizontal to a steep slope with a circular arc transition is modeled. Second, flow over a symmetric and an asymmetric bed profile is tested.

Note that, the utilized **FLOW-3D**[®] applies the True-VOF (volume-of-fluid) technique for treatment of the free surface, and hence, does not incorporate any hydrostatic pressure distribution assumption (i.e. "streamline curvature" explicit consideration) but the utilized version of **NASIR** flow solver which solves depth average flow equations on variable steep slope bed uses hydrostatics pressure distribution assumption [18].

HIS document is a template for *Word (doc)* versions. If you are reading a paper version of this document, so you can use it to prepare your manuscript.

II. GOVERNING EQUATION

A. 3D Flow and VOF Equations

The general mass continuity equation that uses in **FLOW-3D**[®] is:

$$V_f \frac{\partial \rho}{\partial t} + \frac{\partial}{\partial x}(\rho u A_x) + \frac{\partial}{\partial z}(\rho w A_z) = 0 \quad (1)$$

Where V_f is the fractional volume open to flow, ρ is the fluid density. The velocity components (u, w) are in the coordinate directions (x, z). A_y and A_z are similar area fractions for flow in the y and z directions, respectively.

The equation of motion for the fluid velocity components in the two directions are the Navier – Stokes equations (in **FLOW-3D**[®]) as follows:

$$\frac{\partial u}{\partial t} + \frac{l}{V_f} \left\{ u A_x \frac{\partial u}{\partial x} + w A_z \frac{\partial u}{\partial z} \right\} = -\frac{l}{\rho} \frac{\partial p}{\partial x} + G_x + f_x \quad (2)$$

$$\frac{\partial w}{\partial t} + \frac{l}{V_f} \left\{ u A_x \frac{\partial w}{\partial x} + w A_z \frac{\partial w}{\partial z} \right\} = -\frac{l}{\rho} \frac{\partial p}{\partial z} + G_z + f_z \quad (3)$$

In these equations G_x, G_z are body accelerations, and f_x, f_z are viscous accelerations that for a variable dynamic viscosity μ are as follows:

$$\rho V_f f_x = - \left\{ \frac{\partial}{\partial x} (A_x \tau_{xx}) + \frac{\partial}{\partial z} (A_z \tau_{xz}) \right\} \quad (4)$$

$$\rho V_f f_z = - \left\{ \frac{\partial}{\partial x} (A_x \tau_{xz}) + \frac{\partial}{\partial z} (A_z \tau_{zz}) \right\} \quad (5)$$

Where:

$$\tau_{xx} = -2\mu \frac{\partial u}{\partial x} \quad (6)$$

$$\tau_{zz} = -2\mu \frac{\partial w}{\partial z} \quad (7)$$

$$\tau_{xz} = -\mu \left\{ \frac{\partial u}{\partial z} + \frac{\partial w}{\partial x} \right\} \quad (8)$$

$$\tau_{yz} = -\mu \left\{ \frac{\partial v}{\partial z} + \frac{\partial w}{\partial y} \right\} \quad (9)$$

Fluid configuration is defined in terms of a volume of fluid (VOF) function, $F(x, z, \text{ and } t)$. This function represents the volume of fluid per unit volume and satisfies the equation.

$$\frac{\partial F}{\partial t} + \frac{l}{V_f} \left[\frac{\partial}{\partial x} (F A_x u) + \frac{\partial}{\partial z} (F A_z w) \right] = 0 \quad (10)$$

The interpretation of F depends on the type of problem being solved. For a single fluid, F represents the volume fraction occupied by the fluid. Thus fluid exists where $F=1$ and void regions correspond to locations where $F=0$. Voids are regions without fluid mass that have a uniform pressure assigned to them. Physically they represent regions filled with a vapor or gas whose density is insignificant with respect to fluid density.

B. 2D Depth Average Equations on Sloping Bed

The water phase mathematical equations are shallow water equations modified for a coordinate system with an axis normal and two axes (x' and y) parallel to the bed surface (in **NASIR** flow solver).

$$\frac{\partial h'}{\partial t} + \frac{\partial (h' u')}{\partial x'} + \frac{\partial (h' v')}{\partial y} = 0 \quad (11-a)$$

$$\frac{\partial (h' u')}{\partial t} + \frac{\partial (u' h' u')}{\partial x'} + \frac{\partial (v h' u')}{\partial y} + \frac{\partial}{\partial x'} \left[h' \frac{gh' \cos \alpha}{2} \right] = gh' \sin \alpha - gh' S_{fx'} \quad (11-b)$$

$$\frac{\partial (h' v')}{\partial t} + \frac{\partial (u' h' v')}{\partial x'} + \frac{\partial (v h' v')}{\partial y} + \frac{\partial}{\partial y} \left[h' \frac{gh' \cos \alpha}{2} \right] = gh' S_{fy} \quad (11-c)$$

(3) $gh' S_{fy}$

In which:

$$S_{fx'} = \frac{n^2 u' \sqrt{u'^2 + v^2}}{h'^{4/3}} \quad (12)$$

$$S_{fy} = \frac{n^2 v \sqrt{u'^2 + v^2}}{h'^{4/3}}$$

In these equations x' is the axis tangential to the chute slope and y is the same as the y axis in the global coordinate system; u' and v are the velocity components in x' and y directions, respectively; h' is the flow depth perpendicular to the chute bed surface and g is gravity acceleration; α is the chute angle; $S_{fx'}$ and S_{fy} are the bed surface friction slopes in x' and y directions, respectively and n is Manning's friction coefficient [18].

A. 3D Flow Solver with VOF Technique

FLOW-3D[®] numerically solves the equations described in the previous sections using finite-difference (or finite-volume) approximations. The flow region is subdivided into a mesh of fixed rectangular cells. With each cell there are associated local average values of all dependent variables. All variables are located at the centers of the cells except for velocities, which are located at cell faces (staggered grid arrangement). [1]

Curved obstacles, wall boundaries, or other geometric features are embedded in the mesh by defining the fractional face areas and fractional volumes of the cells that are open to flow (the FAVORTM method). [1]

Pressures and velocities are coupled implicitly by using time-advanced pressures in the momentum equations and time-advanced velocities in the mass (continuity) equation. This semi-implicit formulation of the finite-difference equations allows for the efficient solution of low speed and incompressible flow problems. The semi-implicit formulation, however, results in coupled sets of equations that must be solved by an iterative technique. In **FLOW-3D**[®] two such techniques are provided. The simplest is a successive over-relaxation (SOR) method. In some instances, where a more implicit solution method is required, a special alternating-direction, line-implicit method (SADI) is available. The SADI technique can be used in one, two, or in all three directions depending on the characteristics of the problem to be solved. The basic numerical method used in **FLOW-3D**[®] has a formal accuracy that is first order with respect to time and space increments. Special precautions have been taken to maintain this degree of accuracy even when the finite-difference mesh is non-uniform.

A new VOF advection method based on a 3-D reconstruction of the fluid interface has been developed and implemented in **FLOW-3D**[®] Version 8.2. The Volume-of-Fluid (VOF) function is moved in one step, without resorting to an operator splitting technique, which gives the present method increased accuracy when the flow is not aligned with a coordinate direction.

The existing VOF advection method in **FLOW-3D**[®] is based on the donor-acceptor approach first introduced by Hirt and Nichols.

B. 2D Depth Average Flow Solver

NASIR solver uses the shallow water equations. In the numerical model (1&2), the shallow water equations have been modified for a coordinate system with an axis normal and two axes (x' and y) parallel to the bed surface. The depth and velocity values are depth-averaged values computed on a triangular unstructured mesh using the finite volume method. The equations have been converted to discrete form using the overlapping cell vertex and cell centre method. The experimental relations have been added to the model to compute the inception point distance from the crest, the flow depth in this section and the depth-averaged air concentration

in each joint. Then the velocity and air concentration distributions in flow depth have been obtained using experimental relations. Can write the formed vector in before stage the shallow water equations:

$$\frac{\partial Q}{\partial t} + \frac{\partial E}{\partial x} + \frac{\partial F}{\partial y} = S \quad (13)$$

Application of the Green' theorem in equation (13) and the integrated equation form is:

$$\int_{\Omega} \left(\frac{\partial Q}{\partial t} + \frac{\partial E}{\partial x} + \frac{\partial F}{\partial y} \right) dx dy = \int_{\Omega} S dx dy \quad (14)$$

$$Q^{n+1} = Q^n - \frac{\Delta t}{\Omega} \sum_{k=1}^N (\bar{E} \Delta x - \bar{F} \Delta y)_k + S \Delta t \quad (15)$$

Where Ω is the area of the control volume, Q^{l+n} is the value of Q to be computed after Δt and N depend of the finite volume method (overlapping cell vertex and cell centre method).

IV. COMPARISON OF THE NUMERICAL EXPERIMENTS

For the present numerical investigation, the experimental measurements reported by Montes (1994) are used. The experimental data for water-surface and bed pressure profiles obtained from the plots provided by Montes (1994). These experiments were performed in a smooth channel 0.402 m wide. The steep slope 45° was studied. For this slop transition from horizontal to steep slop was obtained through a circular arc of 0.1-m radius.

The model boundary condition for this case, with critical flow occurring at upstream boundary, are specified upstream depth (h_0) and vanishing derivatives of extra pressure and velocity variables. As downstream flow is supercritical, no conditions are applied at downstream end. For this case the bed shear stress term in neglected.

Figs. 1 and 3 show the compute velocity magnitude and pressure counture and Figs. 2 and 4 show the compute and measured water-surface and bed-pressure profiles for different discharges. The model predicted both the water-surface and bed-pressure extremely well. The agreement appears to improve with increasing discharge.

The hydrostatic bed-pressure also shows in Fig. 3. The computed pressure distribution presents little differences with hydrostatic pressure distribution except for transition sections. These differences are due to curved bed in transition and efficiency of centrifugal acceleration.

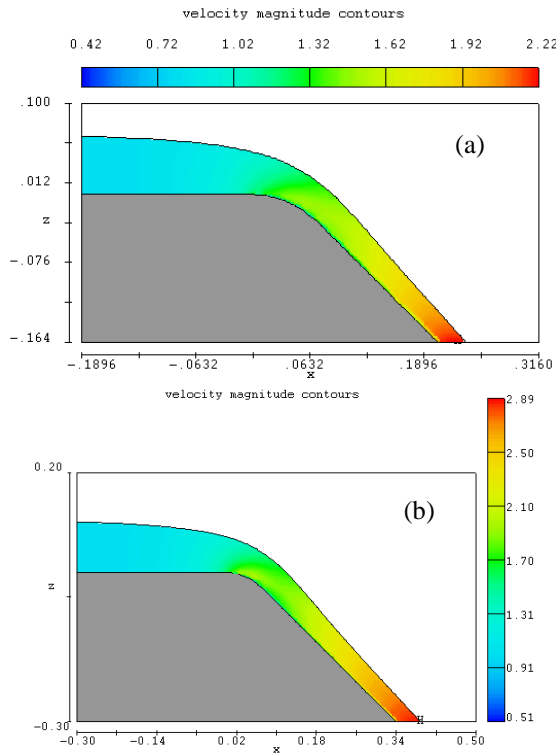


Fig. 1 Computed velocity magnitude contours (m/s) for 45° slop in Flow-3D: (a) $Q=0.02$ m³/s; (b) $Q=0.04$ m³/s.

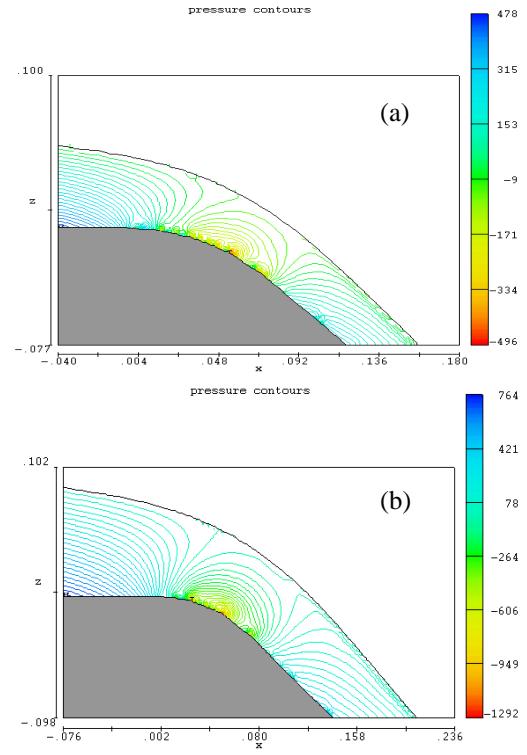


Fig. 3 Computed pressure contours (Pa) for transition 45° slop in Flow-3D: (a) $Q=0.02$ m³/s; (b) $Q=0.04$ m³/s.

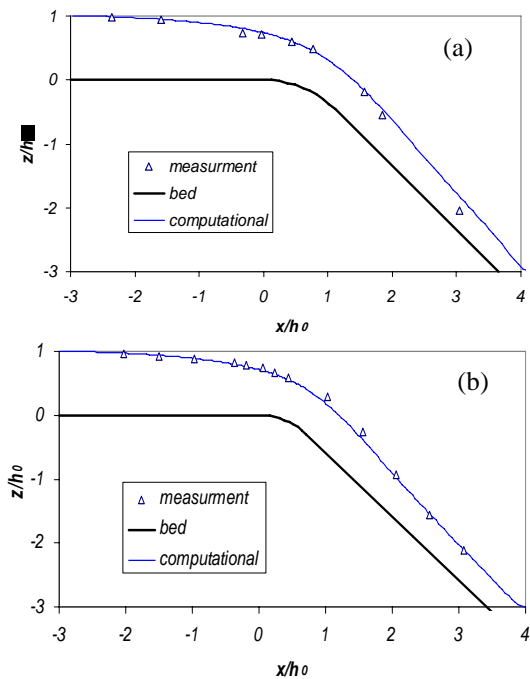


Fig. 2 Water-Surface profile for transition 45° slop: (a) $Q=0.02$ m³/s; (b) $Q=0.04$ m³/s.

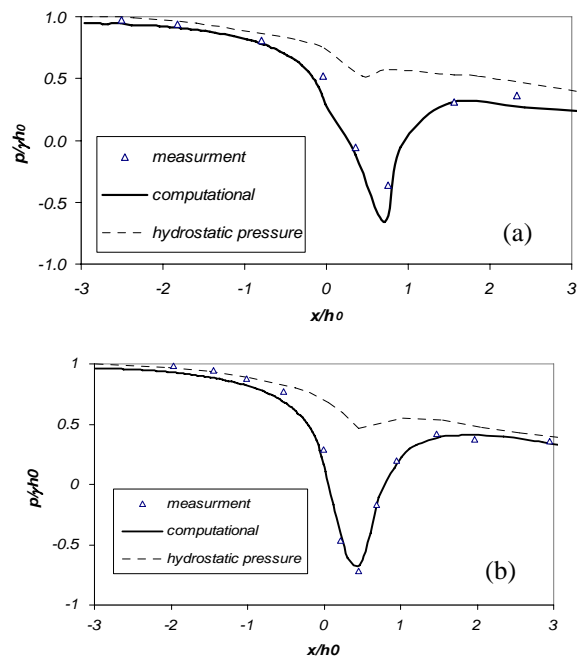


Fig. 4 Bed-Pressure for transition 45° slop: (a) $Q=0.02$ m³/s; (b) $Q=0.04$ m³/s.

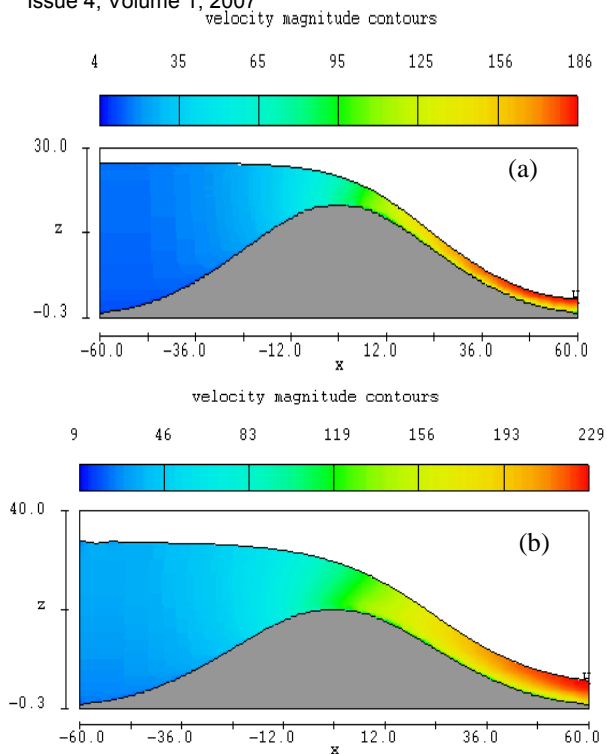


Fig. 5 Computed velocity magnitude (m/s) for symmetric bed in flow-3D: (a) $q=359.9 \text{ cm}^2/\text{s}$, (b) $q=1,119.7 \text{ cm}^2/\text{s}$.

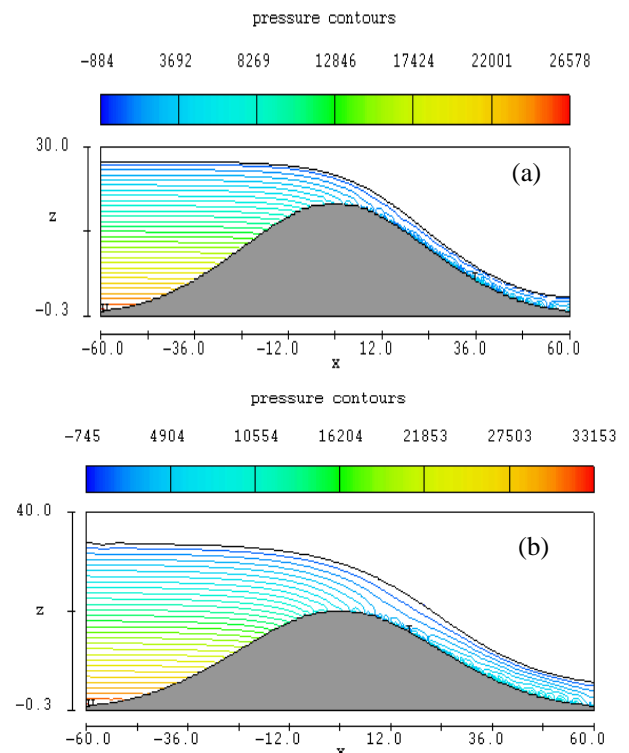


Fig. 7 Computed pressure contours (Pa) for symmetric bed in flow-3D: (a) $q=359.9 \text{ cm}^2/\text{s}$, (b) $q=1,119.7 \text{ cm}^2/\text{s}$.

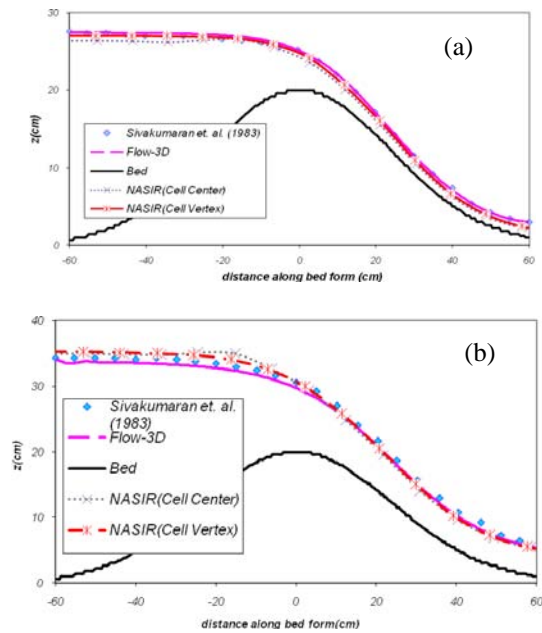


Fig. 6 Water-Surface profile for symmetric bed form: (a) $q=359.9 \text{ cm}^2/\text{s}$, (b) $q=1,119.7 \text{ cm}^2/\text{s}$.

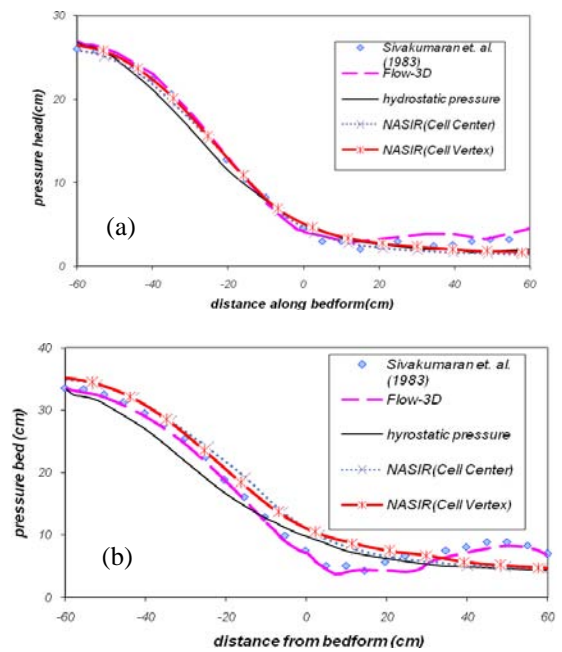


Fig. 8 Bed-Pressure for symmetric bed form: (a) $q=359.9 \text{ cm}^2/\text{s}$, (b) $q=1,119.7 \text{ cm}^2/\text{s}$.

The experimental measurements reported by Sivakumaran et al. (1983) are used for the present numerical investigation. These experiments were performed in a horizontal flume 915 cm long, 65 cm high and 30 cm wide. Two symmetric and asymmetric bed profiles, as shown in Figs. 5 and 9 were tested. The leading edge of profile in each case was placed 366 cm downstream from the inlet box, i.e., head tank. The upstream undisturbed depth was measured at 16 cm from leading edge of profile. The symmetric profile was shaped according to a normal distribution, and was 20 cm high and 120 cm long. The asymmetric profile, with a 150-cm length, was achieved by passing a B-spline through a fixed set of coordinates. Further details of experimental system and bed

The upstream undisturbed depth was measured at 16 cm from leading edge of profile. The symmetric profile was shaped according to a normal distribution, and was 20 cm high and 120 cm long. The asymmetric profile, with a 150-cm length, was achieved by passing a B-spline through a fixed set of

The upstream undisturbed depth was measured at 16 cm from leading edge of profile. The symmetric profile was shaped according to a normal distribution, and was 20 cm high and 120 cm long. The asymmetric profile, with a 150-cm length, was achieved by passing a B-spline through a fixed set of

profile can be found in Sivakumaran and et al. (1983).

The results of *FLOW-3D*[®] and *NASIR* flow solver along with experimental data for the symmetric are shown in Figs. 6 and 8. For the low flow, the predicted water-surface elevation for compare well with the measured data in the sub-critical region, while in the supercritical region the measured data show some scatter that is due to local turbulence resulting matches well with the measured data in the supercritical region, while the results in sub-critical regions follow the hydrostatic pressure distributions. The result of bed pressures from bed curvature, as discussed by Sivakumaran et al. (1983). The pressure deviated from hydrostatic pressure distribution in the high curvature zone and this gap increases for high flow rate. For the high flow rate, the predicted water-surface elevation matches well with the measured data in the supercritical region. For the supercritical region, the model predicts a lower water surface elevation and bed pressure, while oscillations are predicted for both surface elevation and bed pressure just upstream from the crest.

The results of water-surface elevation for cell center model in *NASIR* flow solver matches better than cell vertex model.

The results for the asymmetric shape are shown in Figs. 9-12. For the asymmetric shape, Figs. 11 and 12 show the compute and measured water-surface and bed-pressure profiles for various discharges. The predicted depth and pressure in region of steep slope matches well with measured data if the bed and water surface curvatures are considerably large. However, for higher flow rate the numerical results present better agreements with experimental measurements in the steep slope regions.

In this case the predicted water-surface elevation for cell center model in *NASIR* flow solver is more accurate than cell vertex model.

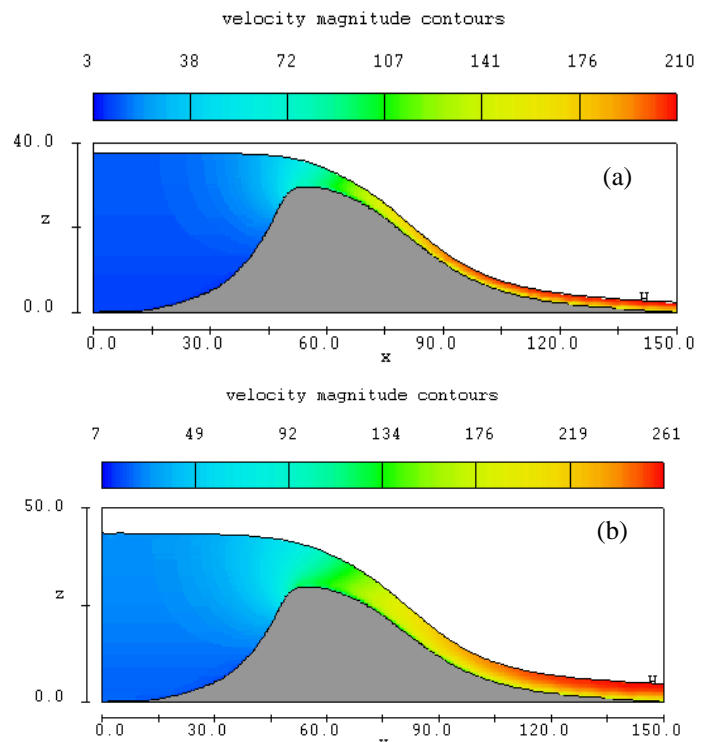


Fig. 9 Computed velocity magnitude (m/s) for asymmetric bed form in flow-3D: (a) $q=375.0 \text{ cm}^2/\text{s}$, (b) $q=1,116.5 \text{ cm}^2/\text{s}$.

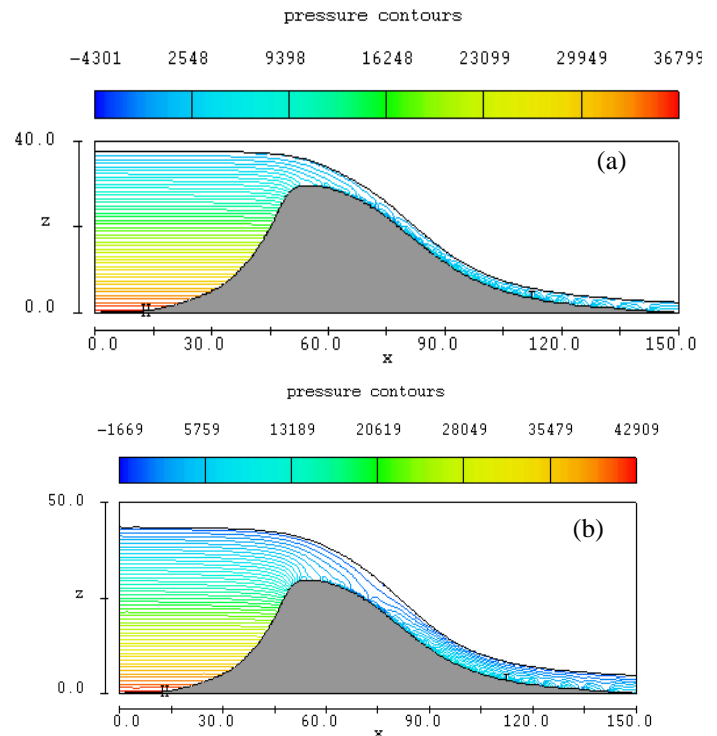


Fig. 10 Computed pressure contour (Pa) for asymmetric bed form in flow-3D: (a) $q=375.0 \text{ cm}^2/\text{s}$, (b) $q=1,116.5 \text{ cm}^2/\text{s}$.

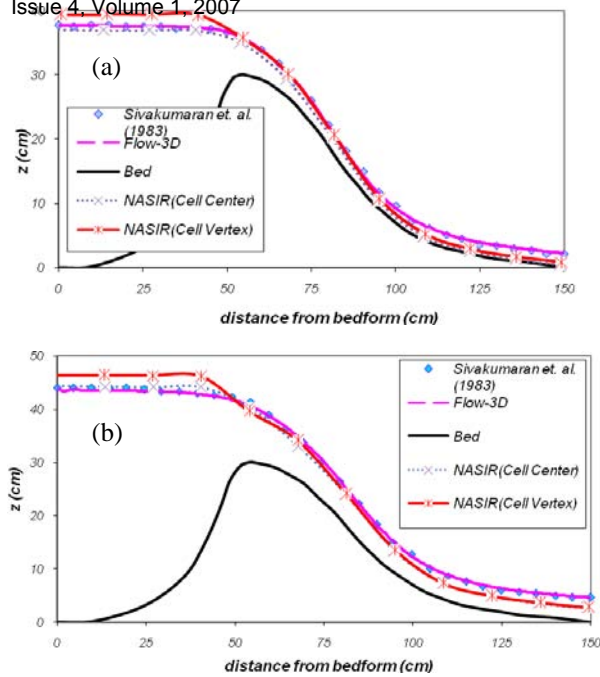


Fig. 11 Water-Surface profile for asymmetric bed form:
(a) $q=375.0 \text{ cm}^2/\text{s}$, (b) $q=1,116.5 \text{ cm}^2/\text{s}$.

V. CONCLUSION

The results of present numerical investigations show that the water-surface elevation computed by both **FLOW-3D**[®] (which uses True-VOF technique for computation of water free surface) and a 2D depth average version of **NASIR** flow solver (which is developed for variable steep slope bed) match well with the measured data.

The computed pressures by the utilized 3D flow solver are in good agreements with the experimental measurements. However, the computed the pressures at the bottom surface of chutes with vertical curvatures slightly differ from the measured pressure in some parts of the super-critical flow parts. The computed pressures along the conduit differ from the hydrostatic assumption due to curved bed and effect of centrifugal acceleration. The differences are more pronounce at the zones with considerably large vertical curvatures, particularly for high flow rates. Therefore, it can be stated that, in the regions with large bottom curvature the pressure distribution does not follow the hydrostatic pressure profile. For the convex bottom curvature the hydrostatic assumption for pressure is more than the actual pressure, while in concave curvature the contrary condition is observed.

REFERENCES

[1] **FLOW-3D**[®] user manual, Ver. 8.2.
[2] C.W. Hirt and B.D. Nichols, "Volume of Fluid (VOF) Method for the Dynamics of Free Boundaries", *J. Comp. Phys.*, Vol. 39, 1981, pp.201-225.
[3] Abdul A. Khan, Peter M. Steffler. "Vertically Averaged and Moment Equation Model for Flow over Curved Beds." *Journal of Hydraulic Engineering*, Vol.122, No. 1, 1996.

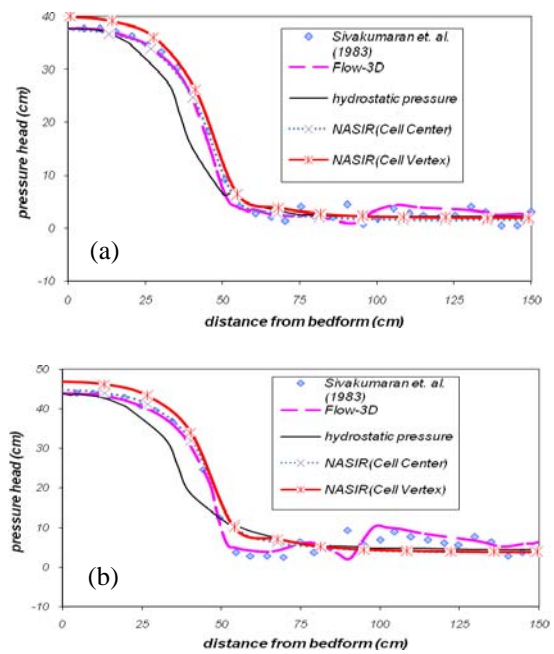


Fig. 12 Bed-Pressure for asymmetric bed form:
(a) $q=375.0 \text{ cm}^2/\text{s}$, (b) $q=1,116.5 \text{ cm}^2/\text{s}$.

[4] J. S. Montes, "Potential-flow solution to 2D transition from mild to steep slope." *Journal of Hydraulic Engineering*, ASCE, Vol. 1(5), 1994, pp. 601-621.
[5] N. S. Sivakumaran, T. Tingsanchali, and R. J. Hosking, "Steady shallow flow over curved beds." *J. Fluid Mech.*, Vol. 128, 1983, pp. 469-487.
[6] V. T. Chow, *Open-Channel Hydraulics*, Mc.Grow Hill Book, 1973, pp.444-448.
[7] R. F. Chaudhry, *Open channel flow*, Prentice-Hall, Englewood Cliffs, N.J. 1993.
[8] R. F. Dressler, "New nonlinear shallow-flow equations with curvature", *J. Hydr. Res.*, Vol. 16, No. 3, 1978, pp. 205-220.
[9] A. M. Gharangik, and M. H. Chaudry, "Numerical simulation of hydraulic jump." *J. Hydr. Engrg.*, ASCE, Vol. 117, No. 9, pp. 1195-1211.
[10] W. H. Hager, "Equation for moderately curved open channel flow." *J. Hydr. Engrg.*, ASCE, Vol. 111, No. 3, pp. 541-546.
[11] W.H. Hager and K. Hutter, "Approximate treatment of plan channel flow." *Acta Mechanica*, Vol. 51, pp. 21-48.
[12] F. Henderson, *Open channel flow*, Macmillan, New York, N.Y.1966.
[13] F. E. Hicks and P. M. Steffler, "Characteristic dissipative Galerkin scheme for open-channel flow", *J. Hydr. Engrg.*, ASCE, Vol. 118, No. 2, 1992. pp. 337-352.
[14] G. D. Mathew, "higher order one-dimensional equations of potential flow in open channels.", *Proc., Institution of Civil Engineers*. London, Englad, Vol. 2(91), 1991, pp. 187-201.
[15] Rao, N. S. L. "Theory of weirs." *Advance in hydroscience*, Vol. 10, 1975.
[16] Steffler, P. M. and Jin, Y. "Depth averaged and moment equations for moderately shallow free surface flow." *J. Hydr. Res.*, Vol. 31, No. 1, 1993, pp. 5-17.
[17] Yen, B. C. "Open channel flow equations revisited." *J. Engrg. Mech. Div.* ASCE, Vol. 99, No. 5, 1973. pp. 99-1009.
[18] Sabbagh-Yazdi SR, Zounemat-Kermani M & Mastorakis EN (2007) "Velocity Profile over Spillway by Finite Volume Solution of Sloping Depth Averaged Flow". *WSEAS Journal of Applied and Theoretical Mechanics*, Issue 3, Vol.2, 85-94.